THEORETICAL AND EXPERIMENTAL STUDY OF A MODEL ROTOR

J-J. Costes , I. Cafarelli , N. Tourjansky
Office National d'Etudes et de Recherches Aérospatiales (ONERA)
92322 CHATILLON CEDEX (France)

Abstract

In this paper , a finite element theory for a rotating beam is presented . The beam can have curvature in every direction of the 3-D space as well as twist . The beam elasticity is represented by the 4 classical stiffness coefficients of extension , torsion , flap and lag . Though the development of the theory is not yet completed , it has already been applied to stability studies for a model rotor in hover . A comparison with experiments carried out in 1988 and 1989 is presented . The tests included variable coupling between the torsion and the second flap modes . The agreement between the theory and the experiments is statisfying .

Introduction

The aeroelastic stability of rotors is still a poorly understood phenomenom . To date , studies concerning this problem , carried out in the Department of Structures at ONERA were based on the classical modal approach [3-6]. Blades were clamped and the first cantilevered modes were measured . Then , by the theory , the effect of centrifugal and aerodynamic forces was introduced . Though this approach was generally sucessful , its drawbacks were important . First of all , either the blade must be built before the modes can be measured or one is obliged to compute the non-rotating modes by some finite element code . For the introduction of the centrifugal forces , a somewhat arbitrary neutral axis on the blade is supposed not to vary in length in spite of all its bending deformations . Another limitation is that the computer programmes are strongly dependant of the mechanical configuration of the rotor hub . All these limitations in the theory and computer codes may be somewhat alleviated if finite elements are used for the blade modeling instead of the non-rotating modes [1-2].

Theory

Development of a beam finite element. The helicopter blade is supposed to be of sufficiently high aspect ratio and thus may be modeled by beam finite elements . The beam approximation is used to replace the actual 3-D problem by a mono-dimentional one . The beam geometry and mechanical properties are allowed to vary along the beam axis . Nevertheless , in the classical beam theory the beam axis is straight and this introduces difficulties if one tries to modelize a highly curved blade such as the blade of a transonic propeller or of an advanced helicopter rotor . The finite element presented in this paper will allow the beam to be curved in all directions of the 3-D space . This introduces also many mathematical difficulties when the displacements are large which is the case at the blade tip , especially for a hinged rotor . To somewhat simplify the problem , as a first step in the theory , the beam mechanical properties are only represented by the 4 classical stiffness coefficients , extension , torsion , flap and lead-lag .

Undeformed finite element . Let us begin by a geometrical description of the undeformed finite element . The reference line is defined by the coordinates $X(v)$, $Y(v)$, $Z(v)$ which are chosen as polynomials of degree 3 of the parameter v varying between 0 and l ; $0 \le v \le l$

$$\begin{aligned} X(v) &= a_0 + a_1 v + a_2 v^2 + a_3 v^3 \\ Y(v) &= b_0 + b_1 v + b_2 v^2 + b_3 v^3 \\ Z(v) &= c_0 + c_1 v + c_2 v^2 + c_3 v^3 \end{aligned} \qquad (1)$$

The coefficients $a_0, a_1, a_2, a_3, b_0, b_1, b_2, b_3, c_0, c_1, c_2, c_3$ give the shape of the reference

line. By analogy with the Bezier's curves , they may be determined by the value of $X(v)$, $Y(v)$, $Z(v)$ and of the tangents $\frac{dX}{dv}$, $\frac{dY}{dv}$, $\frac{dZ}{dv}$ at both extremities for $v=0$ and $v=l$. Other conditions for the determination of the coefficients of (1) are also possible.

At a point P obtained for some value of the parameter v , the tangent to the beam reference line is known . In an absolute reference frame , the direction of this tangent may be given by the 2 angles θ and ϕ (see figure 1) . In figure 1 , Y_L is the tangent to the reference line , OY_2 is parallel to PY_L , ϕ is the angle made by OY_2 with the OXY plane . The projection of OY_2 on OXY is OY_1 . The angle between OY_1 and OX is θ . The direction OX_1 is perpendicular to the direction OY_1 and is on the OXY plane of the absolute reference frame . The directions of PX_2 and of OX_1 are the same . PX_2 is now used to fix the position of the axis PX_L and PZ_L wich are the direction of reference for the description of the local beam section . ψ is the angle between PX_L and PX_2 . $PX_LY_LZ_L$ is the beam local reference frame, its position is given in the absolute reference frame $OXYZ$ by the point P and by the 3 angles θ,ϕ,ψ. The angles θ and ϕ are given by the coefficients $a_1a_2a_3b_1b_2b_3c_1c_2c_3$ of (1) but ψ is arbitrary. The angle ψ may also be chosen as a polynomial of degree 3 of the variable v . The geometry of the undeformed finite element will thus be described by 16 coefficients.

Rigid body displacement . The deformations of an actual helicopter blade are generally small but the displacements may be large , especially at the blade tip . Thus the basic of functions describing the geometrical shape of the deformed finite element must also include large rigid body translations and rotations . In matrix representation , a translation is given by a constant vector and a rotation by a matrix with constant coefficients . The vector or the matrix have thus terms independent of the parameter v . When both transformations are applied to system (1) , the coordinate of the transformed finite element reference line will still be given by polynomials of degree 3 depending on the variable v . Let us assume that the coordinates $X(v)$, $Y(v)$, $Z(v)$ of the reference line after deformation are given by :

$$\begin{aligned} X(v)&=a_0+\bar{a}_0+(a_1+\bar{a}_1)v+(a_2+\bar{a}_2)v^2 \\ &\quad +(a_3+\bar{a}_3)v^3 \\ Y(v)&=b_0+\bar{b}_0+(b_1+\bar{b}_1)v+(b_2+\bar{b}_2)v^2 \\ &\quad +(b_3+\bar{b}_3)v^3 \\ Z(v)&=c_0+\bar{c}_0+(c_1+\bar{c}_1)v+(c_2+\bar{c}_2)v^2 \\ &\quad +(c_3+\bar{c}_3)v^3 \end{aligned} \qquad (2)$$

The 12 coefficients $\bar{a}_0,\bar{a}_1,\bar{a}_2,\bar{a}_3,\bar{b}_0,\bar{b}_1,\bar{b}_2,\bar{b}_3,$ $\bar{c}_0,\bar{c}_1,\bar{c}_2,\bar{c}_3$ are arbitrary constants . All possible polynomials of degree 3 are generated by these coefficients and thus , the rigid body translations and rotations are also included in the set of relations given by (2) . Nevertheless, this is not enough to describe the geometrical shape of the finite element after a rigid body displacement . The new position of the beam sections must also be given . Let us consider only the local reference frame $PX_LY_LZ_L$ at the begining of the finite element ($v=0$) and let us call T the rotation which changes the reference frame from its initial to its final position . T is determined by the initial and final values of the angles θ,ϕ,ψ for $v=0$. Now , in the case of a rigid body displacement , the same transformation T , applied to the initial position of any local reference frame will give its final position . For $0\le v\le l$:

$$(\theta,\phi,\psi)_{final} = T.(\theta,\phi,\psi)_{initial} \qquad (3)$$

The transformation T is not arbitrary , the values of θ and ϕ are also given by the position of the tangent to the finite element reference axis . The angles θ and ϕ can be deduced from the set of equations (2) and must agree with the values given by (3) .

Finite element with deformation: Some simplifying assumptions will be made on the deformation of the beam element . The beam sections remain normal to the beam reference axis after deformation and these sections remain plane and undeformed . The position in the absolute frame of the finite element reference axis is given by the relations (2) where the coefficients $\bar{a}_0.....\bar{c}_3$ can take arbitrary values . This determines the values of θ and ϕ for $v=0$ after deformation . The value of ψ for $v=0$ is arbitrary . The values of θ,ϕ,ψ before and after deformation define the transformation T according to (3) . Before deformation , the transformation T may be applied to any local reference frame . The new

frame obtained will be called the "rigid body local reference frame" . This new frame is used for the determination of the final position of the beam section which is deduced from the rigid body reference frame by 3 rotations of angles α,β,γ .

α is a rotation in the lead-lag direction .

β is a rotation in flap .

γ is a rotation in torsion .

In the case of a rigid body displacement these 3 angles are equal to zero . In the case of a beam with elastic deformations , the angles will remain small and the order in which the rotations occur can generally be overlooked. The angles α and β are determined by the tangent to the beam reference axis after deformation but γ is arbitrary except for the condition $\gamma = 0$ for $v = 0$. The angle γ may be taken as a polynomial of degree 3 of the variable v .

$$\gamma = \gamma_1 v + \gamma_2 v + \gamma_3 v \qquad (4)$$

The geometrical shape of the beam finite element is determined by 16 parameters :

12 coefficients $\bar{a}_0,.....,\bar{c}_3$,

the value of ψ for $v=0$ after deformation ,

3 coefficients $\gamma_1,\gamma_2,\gamma_3$ for the beam torsion .

These unknown parameters will be determined by the equations of elasticity as will be seen later . Though the 16 parameters describe perfectly the geometrical shape of the finite element after deformation , they are mathematical parameters rather than physical ones . For this problem , the physical parameters are the values of $X(v),Y(v),Z(v),\psi(v)$ and their derivatives $\frac{dX}{dv},\frac{dY}{dv},\frac{dZ}{dv},\frac{d\psi}{dv}$ along the finite element .

When the beam is modeled by more than one finite element , special conditions must be written for the physical parameters at the junctions between the elements . Usually , $X(v),Y(v),Z(v),\psi(v)$ are continuous along the beam and sometimes this is also true for the derivatives . When the displacements are large, these conditions give non-linear equations which must be linearized around some starting value and solved by a step by step method .

Elastic energy of the beam finite element .

Let us consider two sections of the beam relative to the parameters v and $v+dv$. The finite element has been defined by means of polynomials which are continuous functions and thus the two reference frames cannot be very different . This is true even after deformation . By a translation and a rotation , let us superpose the two local reference frames obtained for the parameter v before and after deformation . Let us now consider the reference frames before and after deformation for the parameter $v+dv$. The same translation and rotation is applied to the reference frame after deformation of the finite element . This transformed frame is different from the frame before deformation , excepted in the case of a rigid body motion . Nevertheless , both frames cannot be very different because neither differs much from the frames for the parameter v which have been superposed . This small difference can be interpreted as 3 rotations $d\omega_x,d\omega_y,d\omega_z$ which are the bendings and torsion of the beam . When second order terms are neglected , the total transform does not depend on the order of occurence of the 3 rotations .

The extension ε of the beam can be computed by comparing the length before and after deformation of a beam element taken between the values v and $v+dv$ of the parameter defining the reference axis .

The theory presented in this paper is geometrically rather complex , that is why only the classical beam theory for the computation of the virtual work of the elastic forces has been used . In the classical theory , only 4 parameters are considered :

EI_x is the stiffness in flap .

EI_z is the stiffness in the lag direction .

GJ is the stiffness in torsion .

ES is the stiffness in extension .

The virtual work δT due to the elastic forces is given by :

$$\delta T = \delta\left[\frac{d\omega_x}{du}\right] EI_x \frac{d\omega_x}{du} + \delta\left[\frac{d\omega_y}{du}\right] GJ \frac{d\omega_y}{du} + \delta\left[\frac{d\omega_z}{du}\right] EI_z \frac{d\omega_z}{du} + \delta\varepsilon\, ES\, \varepsilon \qquad (5)$$

where u represents the curvilinear abscissa along the finite element reference axis and

may be computed as a function of the parameter v . For the whole finite element , the virtual work is obtained by integrating δT from $v = 0$ to $v = l$. The 4 stiffness coefficients may also depend on v , they may be taken as polynomials of the variable v . The virtual work may be computed for any given combination of displacement and elastic deformation , but it is also necessary to investigate the case of small perturbations around a given initial state. The computation of the virtual work must be carried up to the second order and this is not in agreement with the definition of the 3 rotations $d\omega_x, d\omega_y, d\omega_z$ where second order terms have been neglected . This cannot be avoided in a beam theory . In this way , errors are introduced in the value of the beam elastic energy which will result in small errors in the calculated frequencies of the beam natural modes . These errors will be small by comparison with the errors introduced by the assumptions made for the beam deformation where the sections are supposed to remain perpendicular to the beam reference axis .

Completeness and compatibility . A finite element should satisfy the basic requirements of compatibility between elements and of its completeness [8 p101]. Here , the compatibility is enforced by special equations written at the node between 2 elements . A first set of equations is obtained by the condition of continuity for the 3 coordinates X, Y, Z and for the angular position of the beam section given by the angle ψ. Another set of equations which involves the derivatives of X, Y, Z, ψ is obtained by writting the condition of continuity between 2 elements for the traction force and for the 3 bending and torsional moments . All these equations are generally non-linear , they must be linearized around some starting value of the 16 state parameters of the finite elements . The final solution must be looked for by a step by step method .

For the completeness of the element , two conditions must be satisfied . The first condition is that any rigid body motion will not induce strain into the element . As said previously , the geometrical shape of the transformed finite element is defined by the superposition of a rigid body motion and an actual deformation . Thus in the case of translation and rotation of the whole finite element, there is no deformation . The angles α, β, γ as well as $d\omega_x, d\omega_y, d\omega_z$, the bendings and torsion of the beam are equal to zero. This makes the moments of the forces of flexion and torsion equal to zero in the whole element . Moreover , a rigid body motion does not change the length of the beam reference axis and the extension ε as well as the force $ES.\varepsilon$ are equal to zero all along the beam .

The second condition for the completeness of the finite element states that it should be possible to find a deformation corresponding to a state of constant strain . This condition is not rigorously met by the finite element presented in this paper . Nevertheless , when the length of the finite element is small compared to its curvature and when the stiffness coefficients EI_x, EI_z, GJ, ES , do not vary too rapidly along the element , it is possible to compute a limited expansion in v of the deformation that will satisfy the constant strain condition . If all the terms of degree higher than 3 can be neglected , then the condition is satisfied .

Virtual work of inertia forces. For applications to a propeller or to a helicopter rotor , the beam can have small vibrations around a given deformed state as well as a rotation around the center of the rotor . In the present theory , only a rotation with a constant speed has been considered and there is no vibration of the hub , that is to say no displacement of the rotor center . The rotation of the beam creates constant acceleration forces which induce displacements and deformations of the beam . This inital pre-constrained state must be computed by a step by step method . Let us consider one of the 16 parameters , $\bar{a}_0$ for example . This parameter will be written in the following form :

$$\bar{a}_0 = \bar{a}_{00} + \bar{a}_{01}(t) \qquad (6)$$

where $\bar{a}_{00}$ is a given static deformation of order 0 and $\bar{a}_{01}$ is a static or dynamic deformation of order 1 which is to be calculated . All the 16 parameters $\bar{a}_0 \ldots\ldots \bar{c}_3, \psi(v=0), \gamma_1, \gamma_2, \gamma_3$ are written under a form similar to (6) .
For any point of any section of the finite element , the velocity will be computed up to the 2nd order and the acceleration up to the 1st order in terms of the 16 parameters which define the finite element's deformed state . The virtual displacement can be derived from the expression for the velocity , it is at least of order 1 but terms of the 2nd order also exist . The virtual work of the forces of acceleration is given by the product of the acceleration by

the virtual displacement and it must be evaluated up to the 2nd order . Since the virtual displacement is at least of order 1 , the acceleration needs only to be evaluated up to the 1st order .
The total sum of the virtual work of the elastic and acceleration forces must be equal to zero . This total sum includes terms of 1st and 2nd order . Let us first examine the case of the 1st order terms :
The first part of the 1st order terms comes from the virtual displacement at order 1 multiplied by the steady part of the acceleration which will be denoted by Γ_0 . Other terms come from the virtual work of the elastic forces (5) . In equation (5) , the terms of order 1 of the virtual bendings

$$\delta\left[\frac{d\,\omega_x}{du}\right],\delta\left[\frac{d\,\omega_y}{du}\right],\delta\left[\frac{d\,\omega_z}{du}\right]$$

and of the virtual extension $\delta\varepsilon$ are composed of terms proportional to the 16 virtual deformation parameters $\delta\bar{a}_{01},\delta\bar{a}_{11},.....,\delta\gamma_{31}$. These terms are multiplied by the steady elastic forces E_0 induced into the beam by the steady deformation $(\bar{a}_{00}.....\gamma_{30})$ which is supposed to be of order 0 . Thus the virtual work can be written as :

$$\delta\mathbf{T}_{order\,1} = (\Gamma_0+E_0)\delta\bar{a}_{01} + ... + (.....)\delta\gamma_{31} \quad (7)$$

It is important to note that equation (7) does not include terms proportional to $\bar{a}_{01}.....\gamma_{31}$ or to the derivatives with respect to time such as $\dot{\bar{a}}_{01}.....\dot{\gamma}_{31}$ or $\ddot{\bar{a}}_{01}.....\ddot{\gamma}_{31}$. The terms such as (Γ_0+E_0) are constant and determined by the steady initial conditions .
Now let us examine the 2nd order terms for the total virtual work . The part due to the elastic forces does not include derivatives of $\bar{a}_{01}.....\gamma_{31}$ but the first and second derivatives with respect to time are introduced by the virtual work of the inertia forces . The second order part of the total virtual work can be written under a matrix form such as :

$$\delta\mathbf{T}_{order\,2} = \left[\ \delta\bar{a}_{01}.....\delta\gamma_{31}\right]\left\{\left[\ dM\right]\begin{bmatrix}\ddot{\bar{a}}_{01}\\ \vdots\\ \ddot{\gamma}_{31}\end{bmatrix} + \left[\ dB\right]\begin{bmatrix}\dot{\bar{a}}_{01}\\ \vdots\\ \dot{\gamma}_{31}\end{bmatrix} + \left[\ dK\right]\begin{bmatrix}\bar{a}_{01}\\ \vdots\\ \gamma_{31}\end{bmatrix}\right\} \quad (8)$$

Integration of the virtual work. As seen previously , the first and second order part of the elastic forces' virtual work have been determined for a section whose position on the beam is given by the value of the parameter v. That virtual work depends on the 4 stiffness parameters EI_x, EI_z, GJ, ES and it must be integrated along the whole length of the finite element , that is to say for v varying from 0 to l

For the inertia forces , the first and second order parts of the virtual work must be integrated first over the surface of the beam section and then over the length of the finite element . The surface integration introduces 6 inertia coefficients m, mx, mz, mxx, mzz, mxz which are defined by ;

$$m(v)=\int_{section}\rho dxdz \qquad mx(v)=\int_{section}\rho xdxdz \quad (9)$$

$$mz(v)=\int_{section}\rho zdxdz \qquad mxx(v)=\int_{section}\rho x^2dxdz$$

$$mzz(v)=\int_{section}\rho z^2dxdz \qquad mxz(v)=\int_{section}\rho xzdxdz$$

where ρ is the density by unit length of the finite element . The 6 inertia coefficients must be defined over the whole length of the finite element for the integration with respect to v .

The 3-D mass finite element . For an actual helicopter rotor , small concentrated masses are often placed in the blades to adjust the natural frequencies . With a very good approximation , these masses may be considered as rigid point-like weights . Furthermore , the height z over the surface of the beam can generally be neglected . The inertia forces then depend only on the 3 coefficients m, mx, mxx . Nevertheless , in the applications that will be presented later , the variation of the blade first natural frequency in torsion had to be very large , this has been obtained by means of an inertia arm (fig 3) or by an inertia ring (fig 4) which are very heavy and fully 3 dimensional bodies . For that purpose a special 3-D rigid body element has been developped . For this element (fig 2) , the reference line may be

flexible but the virtual work of the elastic forces is not considered . This virtual work will be taken into account in another normal flexible finite element . At the abscissa v along the reference line , there is a local reference frame X_L, Y_L, Z_L whose position is determined by the deformation of the reference line and the torsion of the element . The 3-D mass is supposed to be rigidly fixed to this reference frame and will move with it . As it can be seen in figure 2 , the 3-D body can have masses outside the $X_L Z_L$ plane. Then , 10 inertia coefficients will participate in the virtual work of the inertia forces . These coefficients are :

$m, mx, my, mz, mxx, mxy, mxz, myy, myz, mzz$.

They are defined by :

$$m = \int_{body} \rho dxdydz \qquad mx = \int_{body} \rho x \; dxdydz \tag{10}$$

$$my = \int_{body} \rho y \; dxdydz \qquad mz = \int_{body} \rho z \; dxdydz$$

$$mxx = \int_{body} \rho x^2 \; dxdydz \qquad mxy = \int_{body} \rho xy \; dxdydz$$

$$mxz = \int_{body} \rho xz \; dxdydz \qquad myy = \int_{body} \rho y^2 \; dxdydz$$

$$myz = \int_{body} \rho yz \; dxdydz \qquad mzz = \int_{body} \rho z^2 \; dxdydz$$

In (10) , ρ is the density of the 3-D rigid body and for more clarity x, y, z have replaced the local coordinates X_L, Y_L, Z_L .

Derivation of the final system. The contributions of all the finite elements which make up the beam must be summed . This gives a second order linear system with a constant right hand side coming from the participation of the 1st order virtual work . There are 16 unknown coefficients $\bar{a}_{01} \ldots \gamma_{31}$ for each finite element in the final system but these coefficients are not independent . As said earlier , the equations of compatibility between the elements must be introduced . These equations are generally non-linear , they will be expanded up to order 1 around the beams initial static deformation defined by the coefficients $\bar{a}_{00} \ldots \gamma_{30}$. The linear relations thus obtained will be used to reduce the size of the second order system . Other relations determined by the mechanical properties of the beam attachment to the rotor hub must also be included . The beam may be clamped or hinged , dampers which may introduce a siffness as well as a damping effect may be present , a coupling between lag and pitch is possible .... All these limit conditions give equations which must be linearized and used in the same way as the compatibility conditions .

Resolution of the system . The first step in the resolution of the second order system is to determine the static part of the solution . For that , only the stiffness matrix is involved . When the right hand side is different from zero , a non-zero incremental deformation is obtained . This solution is added to the initial static deformation and the whole process is repeated up to convergence . The convergence is obtained when the right hand side coming from $\delta \mathbf{T}_{order\,1}$ is sufficiently close to zero to give a negligible increment of the static solution . Once convergence has been attained , the dynamic part of the solution of the second order system can be computed .

First , the second order system is transformed into a first order one by doubling its size . The coefficients $\bar{a}_{01} \ldots \gamma_{31}$ and the derivatives $\dot{\bar{a}}_{01} \ldots \dot{\gamma}_{31}$ are considered as independent parameters . Because only the harmonic solutions are looked for , the relation :

$$\dot{\bar{a}}_{01} = \omega \, \bar{a}_{01} \tag{11}$$

and similar relations for the other variables are also introduced . In (11) , the imaginary part of ω is the circular frequency of the response . The eigenvalues and eigenvectors of the first order differential system are calculated by means of a standard computer code when the size of the system is not too large . The computer code is written for any matrix with complex coefficients and has been used sucessfully with up to 300 variables for this kind of problems . This gives 150 variables to describe the state of deformation of the beam which correspond to approximatively 9 or 10 finite elements .

The frequency ω is a complex number because the damping matrix is different from zero . When there is no dissipation of energy , the damping matrix is still different from zero because of the Coriolis forces but the real part of the frequencies ω is equal to zero . When there is a damper , some of the eigensolutions ω have a negative real part .

Aerodynamic forces . So far , only the computation of the mechanical properties of the rotor

blade have been considered . Nevertheless , the final objective of this study is to determine of the stability characteristics of a rotor in hover . For that purpose , the effect of the aerodynamic forces must be introduced . It is then necessary to define the aerodynamic profile along the blade . For the calculations , only the chord and the position with respect to the local reference frame $PX_L Y_L Z_L$ (fig 1) of the profile's zero incidence axis are necessary.

Many simplifying assumptions have been made in the present theory .

The profile's zero incidence axis is assumed to lie in the $PX_L Z_L$ plane of the local section of the beam .

Only quasi-steady aerodynamics have been considered .

The effect of the spanwise wind (directed along the Y_L axis) is assumed to be negligible .

The first step for the computation of the aerodynamic forces is the determination of the aerodynamic incidence along the rotor blade . This incidence may be computed when the velocity of the points located on the blade reference axis is known . This velocity takes into account the advancing velocity of the whole rotor , the velocity induced throught the rotor disc by the traction forces as well as the vibrations of the blade . Only the two components velocity V_X and V_Z located into the beam local section will be retained . These two components are then projected on the profile zero incidence axis and normally to it . The ratio of these two projections is the tangent of the local aerodynamic incidence . This aerodynamic incidence depends on the initial steady state parameters $\bar{\alpha}_{00}....\gamma_{30}$ and also on the parameters which give the increment of deformation of the blade . These parameters are $\bar{\alpha}_{01}....\gamma_{31}$ and their first derivatives with respect to time , $\dot{\bar{\alpha}}_{01}.....\gamma_{31}$.

For simplicity , only the lift force is considered . Its amplitude is related to the incidence by the classical formula :

$$F = \frac{1}{2}\rho c\,(V_X{}^2+V_Z{}^2)\frac{2\pi\sqrt{1-\eta^2}}{\sqrt{1-M^2}}\alpha \qquad (12)$$

where M is the Mach number , c is the chord, α is the incidence and $\sqrt{1-\eta^2}$ is a correction factor which puts the aerodynamic force equal to zero at both ends of the blade . No drag is added but the direction of the lift is taken as perpendicular to the steady part of the local velocity as it is computed when taking into account only the initial steady state deformation of the beam .

Once the lift force is obtained , the multiplication by the virtual displacement gives the virtual work of the aerodynamic forces . This virtual work is expanded up to order 2 and added to the contribution of the elastic and inertia forces . As said in the previous paragraph , the steady solution is looked for first and this is done by a step by sep method and then the unsteady part of the solution is computed .

The aerodynamic forces introduce terms into the damping matrix of the system of equations. In this case the complex number ω can have a positive or negative real part . The rotor may be stable or unstable .

Experiment

The EDY test rig

A 3 bladed rotor named EDY (**E**tudes **D**ynamiques) was designed and tested in 1988-1989 for rotorcraft aeroelastic stability studies . The rotor diameter is equal to 1.5 m , it is flap-hinged but cantilevered in lag . The maximum rotational speed was approximately 1200 rpm and has recently be pushed up to 2000 rpm . The hub is assumed to be rigid and motionless and this was well verified during the experiments .

Blade design

The blade is straight , rectangular and untwisted with a 5 cm chord . Its stucture has been designed to be very stiff in torsion , it is made of a thin carbon - composite layer covering a polyurethane foam core and an internal beam . It is mass balanced about the fore quarter chord by an inserted inermet spar . The profile shape is a NACA 00016 along the entire blade span .

Root flexure design

The blade is attached to a root flexure as shown in figures 3 and 4 . The flexure has a cruciform cross section which gives a relatively high bending stiffness but a moderately low torsional one . The flexures were dimensioned for the 1st lag frequency to be greater

than the maximum rotational speed in order to avoid ground resonance instabilities . As the blade is very stiff in torsion , the shape of the first torsion mode , when it is mounted on the root flexure , is close to a rigid body motion around the fore quarter chord axis . Its frequency is determined mainly by the stiffness in torsion of the root flexure and by the blade inertia around the fore quarter chord axis .

One of the objectives of the experiments was to study the effect of different degrees of coupling between the torsion and other modes. That is why an easy adjustment of the blade first torsion mode was necessary . This was made by changing the blade inertia in torsion by means of masses located at the blade root to avoid any aerodynamic interactions . Two configurations have been tested . The first (fig 3) , used in the 1988 experiment , had removable masses at both ends of a rigid and light arm lying in the horizontal plane when the blade pitch angle was equal to zero . When the pitch angle was different from zero , the centrifugal forces on the inertia masses acted to reduce the blade pitch . This generated strain in the root flexure . To avoid this phenomenon , in the 1989 experiment the inertia arm was replaced by a light structure where removable inertia rings could be fixed .

Comparison between theory and experiment

The experiments were carried on in 1988 with an inertia arm and in 1989 with an inertia ring . The hover and forward flight cases have been studied with different cyclic and collective pitch angles . Some results were published in [7] . In the present paper , only the hover case with zero pitch angle is considered . Because it is an untwisted blade , there are no aerodynamic forces except those created by the vibrations of the blade . It was experimentally shown that the stability properties of the rotor are mainly determined by the rotor behaviour in hover .

Inertia arm configuration. The rotor is hinged in flap and the bearing axis is not far from the rotor center of rotation . The blade being rather stiff , the frequency of the first elastic flap mode is almost equal to the rotor rotational frequency [fig 5] . For the same reason , the frequency of the lag mode is almost constant in the range of rotational speeds investigated . This freqency is determined by the lag stiffness of the root flexure .

As said earlier , the blade is mass balanced around the fore quarter chord axis and the shape of the first torsion mode is close to a rigid body rotation around this axis , at least for the non-rotating blade . For these reasons , the virtual work of the acceleration forces remains very small for this mode shape and the frequency do not vary much when the rotor speed is increased .

The frequency of the second flap mode (1 node mode) starts from 38.6 hertz for the non-rotating rotor and increases with the rotor speed . The calculations predict that the torsion and the second flap modes have almost the same frequency at a rotational speed of 1200 rpm . In fact , the theory does not predict an actual crossing of the frequency curves but the modes are exchanging shapes very rapidly between 1150 and 1250 rpm (fig 5) . Unfortunately , in that particular experiment , the maximum rotational speed was 1200rpm . Moreover , there were strain gauges only on the root-flexure but not on the blade itself . The strain gauges were responding only to the lag and torsion modes and to the first flap but it was not possible to record the second flap mode . For these reasons , no correlation is possible between the experimental and predicted values of the second flap frequencies . Anyway , small changes in the values of the frequencies of the second flap mode would not modify the overall rotor behaviour . Dampings have been calculated for the flap and torsion modes . They have also been measured for the torsion . The results are shown in figure 6 , they are given as % of the critical damping , that is to say as ratio of the real part over the imaginary part of the complex number ω .

For an isolated torsion mode , a quasy-steady theory predicts zero aerodynamic damping . The damping of the torsion mode then , remains constant and equal to the structural damping when the rotor speed varies . For an isolated flap mode , the aerodynamic forces are proportional to the speed of vibration . This generates a damping well predicted by a quasy-steady theory . When the rotor speed increases , the aerodynamic forces are more important and the damping of the flap mode increases also . For the EDY rotor , in the narrow range of rotational speed where the torsion and flap modes are interacting , the mode shapes are exchanged very rapidly and

this is also true for the frequencies and the dampings . In fact , contrary to what was seen on figure 5 for the frequencies , the theory predicts an actual crossing of the damping curves . This situation is potentially dangerous if the damping of one of the modes becomes too small (or even changes sign) . In this case, the damping of the other mode becomes very large but the rotor is unstable .

For the EDY model , in the inertia arm configuration , the rotor was stable in the range of rotational speed investigated , 0 to 1200 rpm . This was well predicted by the theory as shown in figure 6 . The measurement of the damping was difficult . The modes were excited sinusoidally through the swash plate at the expected regressive mode frequency . The signal was filtered , digitized , processed through FFT , autocorrelated , averaged and stored . The frequencies and dampings were obtained by the well known Moving Block method . It should be noted that this experimental process gives good results for well separated modes with low damping . Errors occur when modes are too close or highly damped . The experimental results for the torsion mode are given in figure 6 . As may be seen on this figure , a very sharp increase in damping occurs at about 1070 rpm. It was conjectured at the time of the experiment that the measured values belong to the torsion mode under 1070 rpm and to the 2nd flap mode over 1070 rpm . Should that explanation be true , some irregularities would be noticeable on the frequency curve . This is not the case . Moreover , sharp pics have also been noticed in the measured dampings for the inertia ring configuration (fig 10-b , 12-a , 12-b) . For these pics , the ratios of the mode frequency to the rotational frequency are : 3.42 , 3.35 , 3.21 , 3.40 . The ratio average value is 3.345 . This is suspiciously close to $3\frac{1}{3}$. The EDY model is a 3 bladed rotor studied here in hover with a pitch angle equal to zero . This means that the wakes of the blades remain in the rotor plane . When a vibration is at the third harmonic of the rotational speed , a given profile receives a maximum of aerodynamic influence from the immediately preceding blade . In fact , the phase of the induced velocity must be taken into account and the effect may be maximum at a frequency close but slightly different from the third harmonic . Moreover , non-linear effects may lock the phenomenum on a sub-harmonic of the rotational frequency . During the experiment , the rotor was noticed to respond to the harmonics of the rotational speed , to the half harmonics and to the harmonics $\pm\frac{1}{3}$. Even without excitation of the model , there was some response at frequencies equal to :

$$n\,fr \quad \frac{2n+1}{2}fr \quad \frac{3n+1}{3}fr \quad \frac{3n+2}{3}fr \qquad (13)$$

where fr is the frequency of rotation of the blade and n is a null or positive integer .

Inertia ring configuration . During the 1988 experiment , some difficulties appeared when it was tried to increase the collective pitch angle . The masses at both ends of the inertia arm were relatively important and when the collective pitch is increased , the masses come closer to the rotor axis of rotation . The effect of the acceleration forces on the masses is to push them away and then to decrease the pitch angle . This generates a high level of stress in the root flexure but has also an important stabilizating effect as it will be seen later . To avoid the high stresses , a more symetrical configuration has been choosen for the 1989 experiment . Now , the frequency of the first torsion mode is adjusted by ring shaped masses . The center of the rings is on the fore quarter chord axis (fig 4) . As far as the theory is concerned , this configuration is more complex . The special shape of the the inertia body has rendered necessary the developpement of the 3-D rigid mass finite element (fig 2) . As seen in figure 4 , the inertia ring is attached by a light structure to one tip of the root-flexure . Nevertheless most part of the total mass is concentrated into removable rings . The rings are closer to the rotor axis of rotation than the root-flexure tip .

For the 1989 experiment some improvements were also made in the design of the hub . The bearings were made stronger so the maximum rotational speed of the rotor could be pushed up to 1800 rpm . Three cases were studied . For the first one , the inertia ring is not very heavy and the frequency of the first torsion mode is high (about 110 hertz) . No coupling with the 2nd flap mode can occured in this case , at least within the authorized range of rotational speed . For the third case , the frequency of the torsion mode is low and a strong coupling with the 2nd flap mode is

expected . The second case is intermediate between the first and the third ones .

First case (no coupling). The theoretical and experimental results are given in figures 7 and 8 . The measurements have been made for the torsion and for the second flap mode . For the frequencies , the agreement with the theory is very good . For the dampings , the discrepancies are more important but the agreement is still quite acceptable . The theory predicts that the rotor is stable in the authorized range of rotational speed and this was confirmed by the experiment .

Second case (intermediate coupling). In this case , the frequency of the first torsion mode is lowered down to about 76 hertz . The torsion interacts with the 2nd flap mode toward 1500 rpm (fig 9) . The results given by the theory and the experiment are shown in figures 9 and 10 a-b . As it may be seen in figure 9 , for the frequencies the agreement is good in spite of some irregularities in the curve relative to the second flap mode . One possible explanation is the influence of the random exitations existing at all the harmonics and at some sub-harmonics of the rotor rotational frequency (see 13) . The figure 10-a presents the results obtained for the damping of the first torsion mode . Both the theory and the experiment show higher damping when the rotational frequency is increased but the theory predicts less damping that have been measured. As noted earlier , this may be explained by the simplifications introduced by a quasy-steady aerodynamic theory . The damping of the second flap mode is given in figure 10-b . The theory shows , first an increase of the damping up to about 1200 rpm and then a decrease for higher rotational speeds . The damping of this mode becomes equal to zero at 1760 rpm and the rotor is unstable at higher speed . As it may be seen in figure 10-b , the theory predicts very accurately the onset of the instability . The fact that the rotor could be unstable was a surprise because the inertia ring configuration was not believed to change much the behaviour of the rotor . In the inertia arm configuration the rotor was stable . Later calculations have shown that masses in the plane of the rotor disc have a stabilizing effect and masses outside of this plane are destabilizing .

The experimental results given in figure 10-b for rotational speeds lesser than 1200 rpm are much greater than the theoretical ones . Part of the discrepancies may come from errors introduced by the Moving Block analysis which does not work well for highly damped modes . Nevertheless , this cannot explain the irregularities in the experimental results . For the damping of the second flap mode , isolated maxima may be seen at 1000 rpm and at 1530 rpm . For the maxima , the ratios of the 2nd flap mode frequency to the rotor rotational frequency are 3.35 and 2.82 . These ratios are close to $3\pm\frac{1}{3}$. There is also a minimum at 1260 rpm which corresponds to the harmonic 3 of the rotational frequency . No pics are obvious in the damping of the torsion mode (fig 10-a) . The frequency of this mode is high enough (over 75 hertz) and the rotational speed corresponding to the third harmonic is 1500 rpm . At that speed , the aerodynamic damping of the torsion mode is important and may render the "harmonic 3" effect less conspicuous .

Third case (strong coupling). For this case , the frequency of the torsion has been lowered to 49 hertz when there is no rotation . The interaction with the 2nd flap mode occurs at a lower rotational speed . In fact , both modes are never very far apart . This is true even when there is no rotation . Now , the interaction of the two modes is more progressive than in the previous cases . The results , for the frequencies , are shown in figure 11 and there is an excellent agreement between the theory and the experiment . The figures 12-a and 12-b shows the results for the dampings . As in the previous case , the rotor is unstable at high rotational speed . The damping of the 2nd flap mode is equal to zero at 1100 rpm and this is well predicted by the theory .

The experimental results for the dampings of the two modes show sharp pics . For the 2nd flap mode , there is a pic at 840 rpm which corresponds to harmonic 3.21 . For the torsion mode , there is a pic at 900 rpm corresponding to harmonic 3.40 . These values are close to $3\frac{1}{3}$. For the torsion mode , the large values at 1050 rpm may correspond to the third harmonic .

Conclusion

In this paper , a finite element beam theory has been presented . The theory is not restricted to the case of a straight beam . The

reference axis of the beam can have twist in all the three spatial dimensions but the beam elasticity is only represented by the four classical stiffness coefficients , extension , torsion, flap and lag . The complex twist of the beam introduces many difficulties in the theory because there is no obvious set of functions which may be used as a basis for the deformations of the finite elements . Moreover, at the blade tip , very large displacements are possible , especially when the blade is articulated in flap . These very large displacements without deformation must be included in the basic functions . For the present theory , the finite elements compatibility conditions are enforced by special non-linear equations written at the nodes . The first completeness condition stating that any rigid body displacement, however large it may be , do not induce strain into the element is exactly met . The second completeness condition is only partially fullfiled . However , when the length of the finite element is small compared to its curvature , it is possible to find a deformation satisfying approximately the constant strain condition .

The theory has been applied to the case of a 3 bladed rotor model in hover . The rotor has a diameter equal to 1.5 m , it is flap-hinged but cantilevered in lag . The frequency of the blade torsion mode can be adjusted by an inertia body placed at the root of the beam . The main objective of the experiment was to study the effect on the rotor stability of various degrees of coupling between the torsion and the second flap modes . In the computations , only quasy-steady aerodynamics have been considered . The results given by the theory have been compared with the experiments carried out in 1988 and 1989 . In the 1988 experiment , the blade torsion frequency was adjusted by masses placed at both tips of an inertia arm . In this configuration the rotor was stable . In the 1989 experiment , the torsion frequency could be changed by means of ring shaped masses . For this new configuration , the rotor was unstable at high rotational speed . The onset of instability was dependent on the degree of coupling between the torsion and the flap modes . Both the mode frequencies and the onset of instability were well predicted by the theory . The agreement was not so good for the dampings , the experiments having been plagued by the random aerodynamic excitations existing at a frequency roughly equal to three times the blades rotational frequency .

References

1 - Hodges D.H , *Non linear equations for dynamics of pretwisted beams undergoing small strains and large rotations* . Nasa TP 2470 , AVSCOM TP 84.A.5 . May 1985 .

2 - Rosen A , Friedmann P.P , *The non linear behaviour of elastic slender straight beams undergoing small strains and moderate rotations* . J. Applied Mech. Vol 46 no 1 March 1979 pp161-168

3 - Tran C.T , Twomey W , Dat R , *Calcul des caractétistiques dynamiques d'une structure d'hélicoptère par la méthode des modes partiels* . La Recherche Aérospatiale 1973-6

4 - Tran C.T , *Stabilité dynamique d'un rotor bipale* . La Recherche Aérospatiale 1978-1

5 - Costes J-J , Nicolas J , Pétot D , *Stability study of a tilt rotor aircraft model* . La Recherche Aérospatiale 1982-6

6 - Pétot D , Besson J-M , *Comportement dynamique d'un "prop-fan"* .Symposium on Aérodynamics and Acoustics of Propellers . AGARD/FDP , October 1-4 , 1984 . Toronto , Canada .

7 - Caffarelli I , Costes J-J , *Measurements and predictions of rotor stability* .3rd Rotorcraft Dynamics workshop . March 7-14 , 1990 . Duke University Durham , North Carolina .

8 - Bathe K.J , *Numerical methods in finite element analysis* . 1976 . Prentice-Hall Inc. Englewood Cliffs , New Jersey .

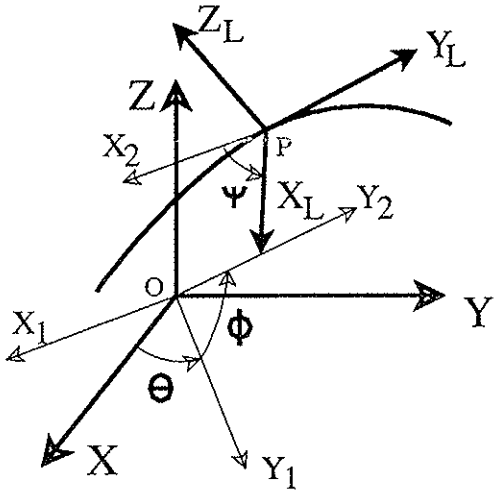

fig 1. Flexible finite element and associated reference axis.

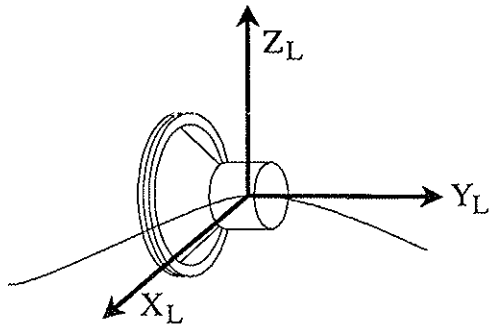

fig 2. Finite element for a 3-D rigid mass

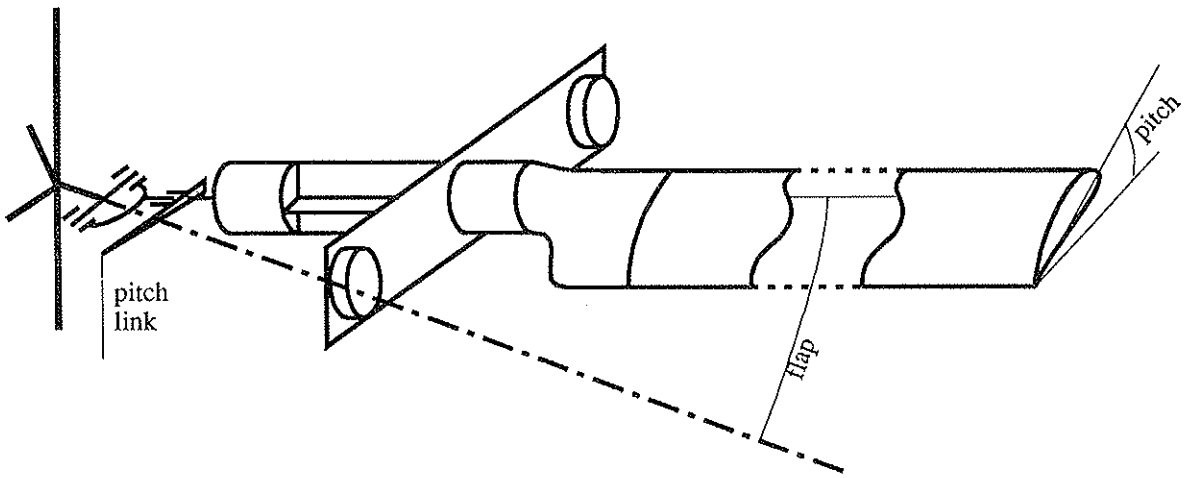

fig 3. Schematic outline of the EDY test rig in the 1988 configuration with an inertia arm supporting adjustable masses .

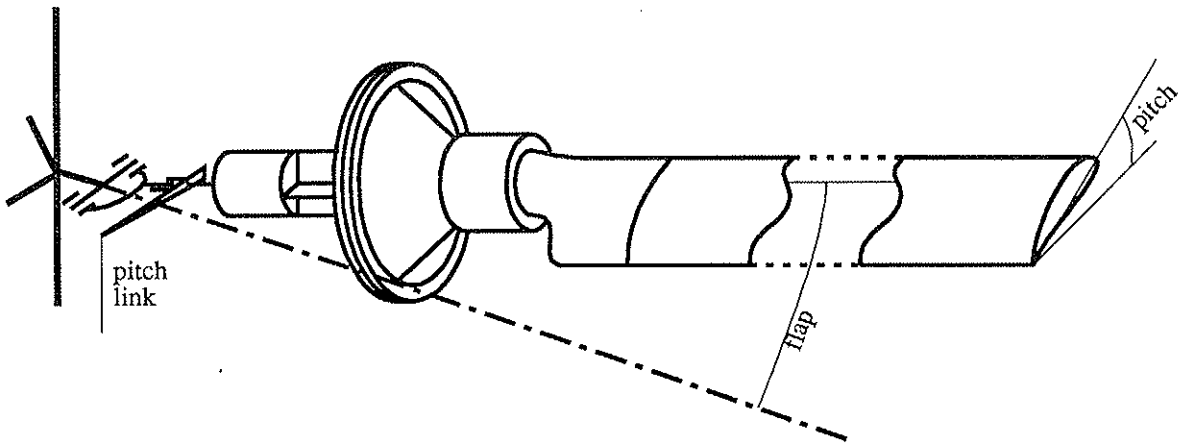

fig 4. Schematic outline of the EDY test rig in the 1989 configuration with an adjustable inertia ring.

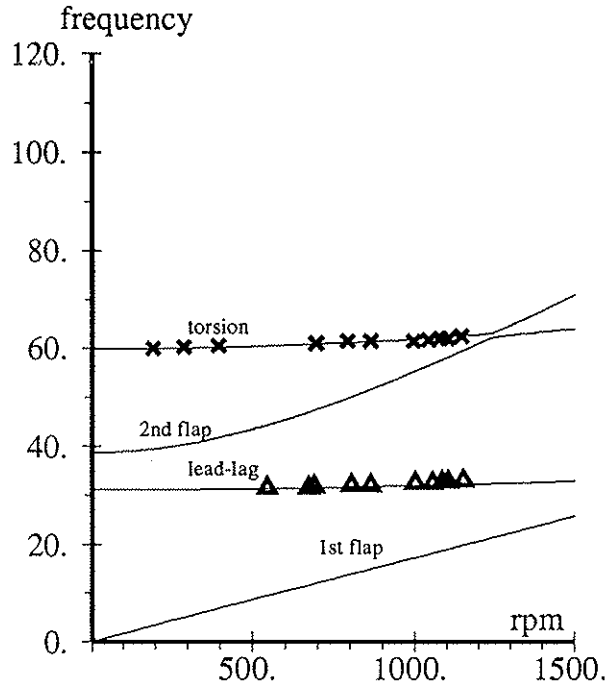

Theory
× Experiment torsion mode
△ Experiment lead-lag mode

fig 5 . EDY with inertia arm
Case with two 24.8g masses

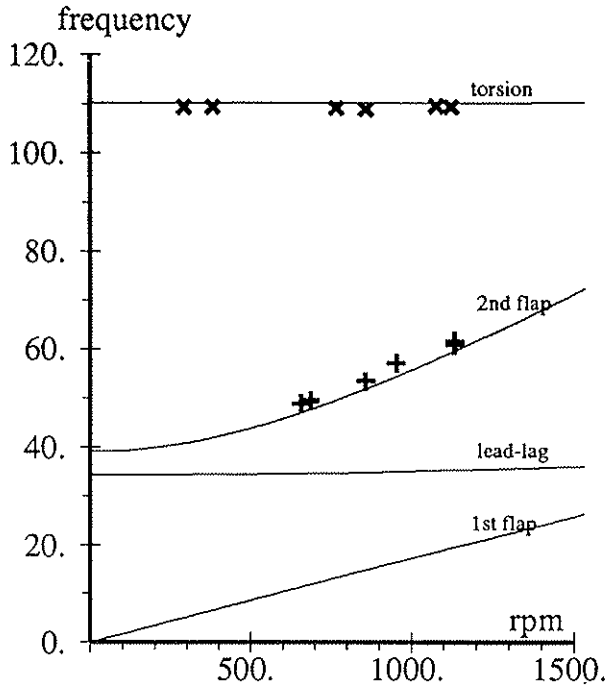

Theory
× Experiment torsion mode
+ Experiment second flap mode

fig 7 . EDY with inertia ring (2mm thick.)
Case without coupling .

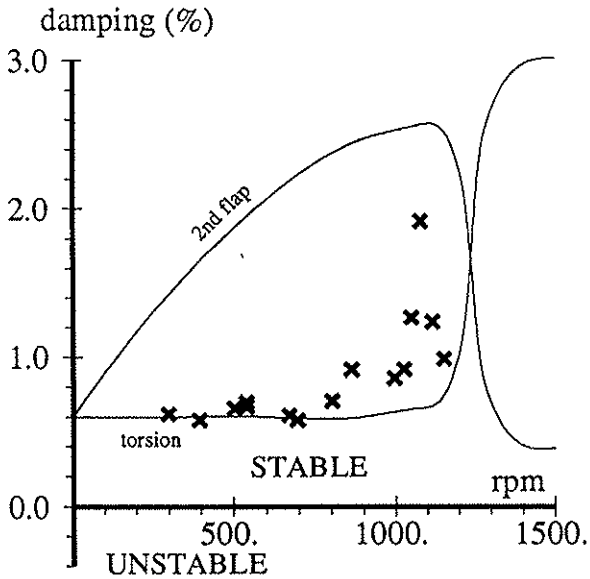

Theory
× Experiment torsion mode

fig 6 . EDY with inertia arm
Case with two 24.8g masses
Damping given as % of critical damping .

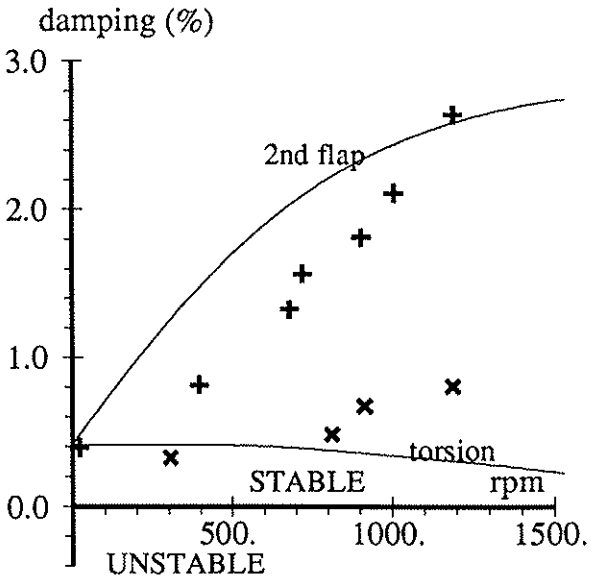

Theory
× Experiment torsion mode
+ Experiment second flap mode

fig 8 . EDY with inertia ring (2mm thick.)
Case without coupling . Damping
given as % of critical damping .

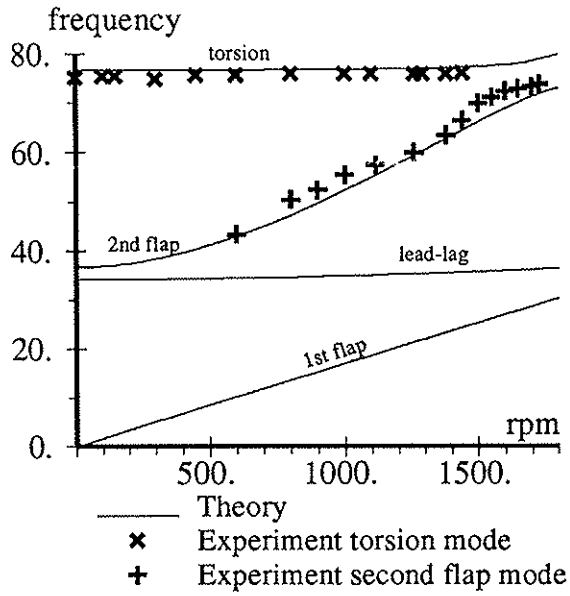

fig 9 . EDY with inertia ring (3mm thick.)
Case with intermediate coupling .

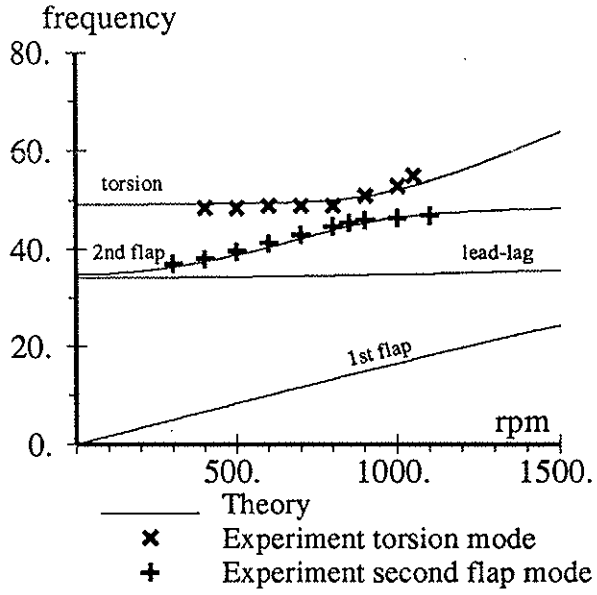

fig 11. EDY with inertia ring (13mm thick.)
Case with strong coupling .

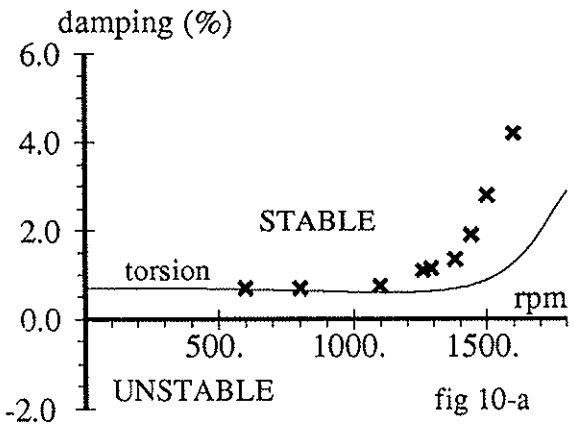

fig 10-a

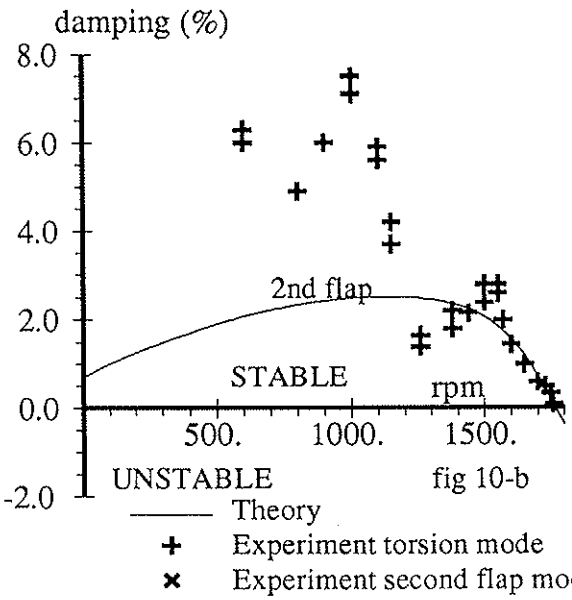

fig 10-b

fig 10 a-b . EDY with inertia ring (3mm thick.)
Case with intermediate coupling . Damping given as % of critical damping .

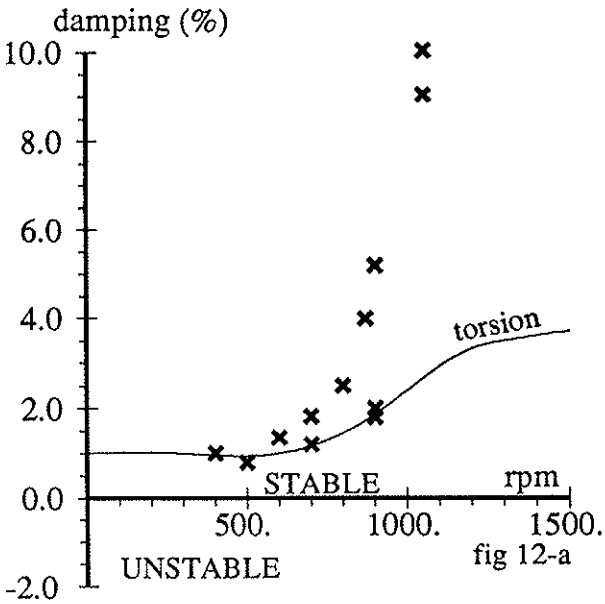

fig 12-a

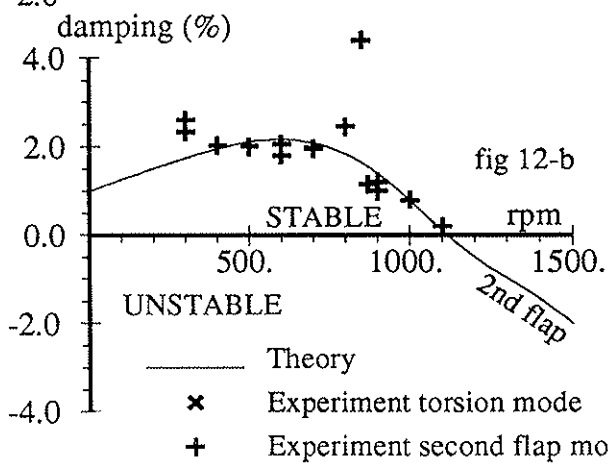

fig 12 a-b . EDY with inertia ring (13mm thick.)
Case with strong coupling . Damping given as % of critical damping .